



Revolutionizing Water Hyacinth Flash Graphene Technology to Remove Cu(II) from Wastewater: Equilibrium Isotherm, Kinetics and Thermodynamic Studies

Amjed Sabah Kamil Janabi^{1,2*}, Hayder M. Abdul-Hameed¹

¹ Departments of Environmental Engineering, College of Engineering, University of Baghdad, Baghdad 10071, Iraq

² Republic of Iraq Ministry of Construction and Housing, Municipalities and Public Works, Baghdad 10071, Iraq

Corresponding Author Email: amjad.Sabah2311@coeng.uobaghdad.edu.iq

Copyright: ©2025 The authors. This article is published by IIETA and is licensed under the CC BY 4.0 license (<http://creativecommons.org/licenses/by/4.0/>).

<https://doi.org/10.18280/ij dne.200206>

ABSTRACT

Received: 10 January 2025

Revised: 16 February 2025

Accepted: 24 February 2025

Available online: 28 February 2025

Keywords:

adsorption, isotherm, kinetics, thermodynamic, flash graphene, copper, Cu(II)

The work examines how flash graphene made from Water hyacinth after flash joule heating (WHAF) behaves as an adsorbent for removing Cu(II) ions from water solutions emphasizing its potential for sustainable and economical use. Broken water hyacinth weeds were subjected to carbonization and electro-flash treatment before being converted into flash graphene. FTIR, SEM, XRD, and BET analyses indicated that water hyacinth after flash joule heating (WHAF) transformed untreated water hyacinth before flash joule heating (WHBF) into an adsorbent with enhanced surface area, improved porosity, and an improved crystalline structure. The study evaluated Cu(II) removal effectiveness under various conditions during batch adsorption experiments, which tested pH values, adsorbent amounts, contact duration, initial metal concentration, speed of agitation, and operating temperature. Cu(II) removal reached its maximum level of 92.09% under pH conditions of 7 and through usage of 1 g of adsorbent for 60 minutes at 45°C. The adsorption process showed heterogeneous energy distribution patterns, which fit both the Freundlich isotherm and pseudo-second-order kinetic models. The sorption process remains stable due to the positive entropy and endothermic nature indicated by thermodynamic analysis. The study demonstrates that WHAF presents feasible economic prospects for eco-friendly heavy metal wastewater remediation while promoting sustainable environmental pollution control. The research findings demonstrate that WHAF can effectively function as an adsorbent material for environmental cleanup.

1. INTRODUCTION

Living organisms on Earth need water as an essential natural resource, which determines their sustainability [1]. In recent years, the growing impact of heavy metals pollution on both terrestrial and marine wildlife has garnered increasing attention, driven by the expansion of modern industries [2]. Exposure to heavy metals has been linked to various health complications in humans and other living organisms [3].

Such pollutants get into the organs and tissues of living organisms by means of water and food contaminated with them. Aquatic environments receive heavy metals through various human activities, including agriculture, industrial processes, urban development, metallurgical operations, use of fossil fuel and utilization of metal pipes, among others [4-7].

Stressful environmental impacts appear from heavy metals that exceed a specific gravity of five, given their characteristics [8]. Thus, heavy metals such as lead (Pb), arsenic (As), zinc (Zn), cadmium (Cd), mercury (Hg), copper (Cu(II)), chromium (Cr), and iron (Fe) infiltrate aqueous bodies in the environment and cause devastating effects on water, air, and soil [9].

Heavy metals toxicity can be roughly ranked in descending

order as $Hg > Cd > Cu(II) > Zn > Ni > Pb > Cr > Al > Fe$. However, this classification approximates, as the sensitivity of different species to specific metals varies. Furthermore, toxicity is influenced by environmental factors that regulate the chemical forms and speciation of these metals [10].

Heavy metals are heavily toxic to human health and their over concentration in biological systems has been linked with lots of health implications. Elevated levels of heavy metals can actually impair one's mental and central nervous system functions and damage vital organs such as the lungs, kidneys, liver, and blood, according to studies. In fact, long exposure time to contaminated wastewater containing toxic heavy metals has been linked to serious conditions such as muscular dystrophy, Alzheimer's disease, different cancers, and multiple sclerosis [11, 12].

However, prolonged exposure in toxic heavy metal wastewaters may cause diseases such as muscular dystrophy, Alzheimer disease, various types of cancer, and multiple sclerosis [13], advanced oxidation [14], flocculation [15], adsorption [16], membrane separation [17], and photocatalytic degradation [18]. Adsorption has been widely applied for this purpose in removing and treating heavy metals from wastewaters [19].

Research has identified lignocellulosic materials as

favorable solutions for the removing of heavy metals from water [20]. Water hyacinth's high cellulose content, with its hydroxyl groups, enhances adsorption by interacting with pollutants, while its porous structure increases surfaces area, making it a cost-effective material for wastewater treatment [21].

These materials offer significant benefits due to their natural abundance, enabling the production of low-cost adsorbents with minimal economic impact [22, 23].

Water hyacinth (WH), an aquatic free-floating plants native to the Amazon Basin, has rapidly proliferated worldwide [24]. This plant is recognized for its rapid growth and its adverse effects on aquatic environments, such as obstructing light penetrating and reducing dissolved oxygen levels, which harm aquatic organisms [25]. With its high cellulose content, comprising approximately 25% cellulose, 33% hemicellulose, and 10% lignin, WH is a valuable natural resource for environmental remediation [26].

Water pollution caused by the red tide affects all aquatic transportation systems as well as hydroelectric plants and the fishing industry [27, 28]. Watery areas infected by WH serve as breeding sites where both snails and mosquitoes transmit diseases to humans [29].

The water hyacinth shows exceptional performance as an environmental pollution control agent because it uses adsorption to remove organic compounds and heavy metals along with water nutrients from polluted water. Its quick reproductive ability combined with large biomass production makes water hyacinth an excellent choice for water cleaning activities. The swift propagation of water hyacinth causes environmental imbalances involving oxygen depletion as well as nutrient disturbances across tropical and subtropical areas. Additional research needs to be performed to identify the right amount of water hyacinth cultivation that preserves environmental stability [30].

The economic use of water hyacinth generates two major benefits including biofuel creation through bioethanol and biodiesel production as well as bioplastic generation. The availability of both cellulose and lipid content in water hyacinth enables it to serve as a sustainable source of materials. Large-scale farming of water hyacinth remains limited at present which restricts its accessibility and requires sustainable sourcing procedures to be established [31].

First it is necessary to investigate how pre-treatment methods can maximize biofuel extraction while determining applications in bioremediation and activated carbon production. Constructing water hyacinth-based wetlands creates opportunities for enhanced wastewater treatment that removes emerging pollutants. Standardized production of water hyacinth presents a sustainable commercial opportunity to control pollution effectively [32].

The WHAF process heat-treats cellulose rapidly to produce a graphene structure, which creates an enlarged surface area and better adsorption qualities. The enhanced pollutant absorption capabilities of graphene through WHAF treatment render it as an environmentally friendly and affordable solution for water filtration and environmental renewal operations than activated carbon, biochar, and nanomaterials [33].

This research aims to analyze the water hyacinth flash graphene form (WHAF) as an adsorbent for removing Cu(II) ions from synthetic aqueous solutions. The adsorbent surface was analyzed through BET surface area measurement and scanning electron microscopy (SEM), X-ray diffraction

(XRD), and Fourier transform infrared spectroscopy (FTIR) to show Cu(II) adsorption. The laboratory procedure involved testing Cu(II) adsorption under different conditions by running batch reactions as a way to examine contact time variations along with adsorbent dosage changes and sample pH control and agitation speed evaluation. The research examines isothermal adsorption together with kinetic and thermodynamic properties to gain better insight into the adsorption process.

2. MATERIALS AND METHODS

2.1 Materials

The researchers obtained WH samples from Euphrates River at Al Kut city within Iraq. The researcher manually cleaned the WH followed by washing it with tap water to eliminate surface sand and unwanted components. After washing the WH were dried under direct sunlight and the lab-scale crusher helped cut them into smaller sizes before placement in clean sealed plastic containers. The collecting process of fresh WH stalks and leaves occurred while omitting the roots to avoid heavy metal accumulation [34].

2.2 Synthesis of flash graphene from water hyacinth

To produce a local adsorbent WH were subjected to a physical activation process where firstly the wastes were carbonized by using a furnace under 250°C for 1hr, and inert condition by pumping CO₂ at rates of 1 L/min, the activation process was activated for WH by the temperature to 150°C in the presence of N₂ at rates of 1L/min for 1hr, and generated (WHBF) [35].

With electro-flash reactor, an electro flash process was used to synthesize flash graphene (WHAF) from crushed water hyacinth derived activated carbon (WHBF). This reactor is key parameters electrode copper, Pyrex tube, voltage 460 × 4 volts, discharge time all 2 second, LED luminaires, capacitor cabinet, circuit breaker, circuit breaker, resistor. Once all cap is charged, it releases energy in a discharge and forms the flash.

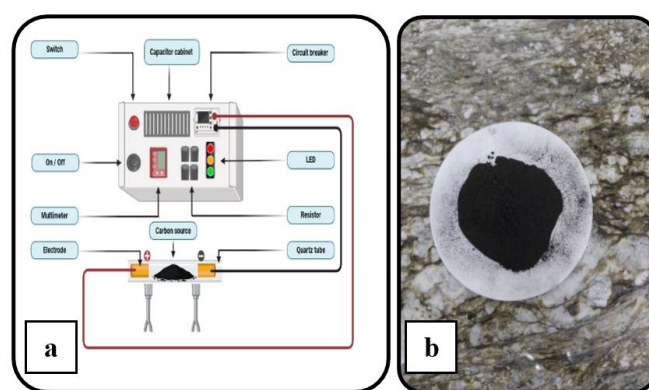


Figure 1. a) Flash graphene synthesized, b) Sample of flash graphene

The step is to put a 5-gram sample of activated carbon into the Pyrex tube and make sure that the copper wire in the tube makes contact with the two metallic electrodes. The bursts of light are triggered at intervals of 2 seconds by a manual circuit break, and 8 to 10 of them are used to drive conversion. The

transformation of the activated carbon into graphene is enabled by each burst. The accompanying schematic diagrams of Figure 1(a), Figure 1(b), and Figure 2 show how this method uses high energy light bursts produced to effectively make graphene from an activated carbon [36, 37].

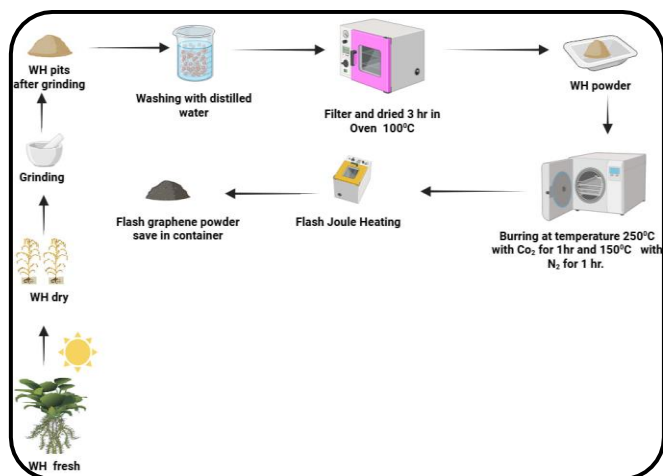
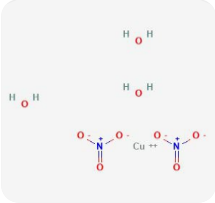


Figure 2. Preparation of flash graphene for heavy metal removal from aqueous solutions

2.3 Preparation of Cu(II)

This study obtained copper nitrate trihydrate ($\text{Cu}(\text{NO}_3)_2 \cdot 3\text{H}_2\text{O}$) from scientific equipment suppliers in Bab Al-Moatham markets, Baghdad, Iraq, with a purity of over 99.9%. The preparation of copper (II) used 1000 mg/L stock solution production through cupric chloride anhydrous dissolving in deionized water followed by creating dilutions at the desired concentration. The stock solutions required further dilution to reach the needed concentration. The prevention of Cu(II) precipitation can be achieved when the solution starting pH remains below 9 [38, 39]. The characteristics of copper (II) ions are presented in Table 1.

Table 1. The main effects and permission limits of some heavy metals

Property	Cupric Nitrate Trihydrate
Phase	Solid, bluish crystals, odorless
Molecular formula	$\text{Cu}(\text{NO}_3)_2 \cdot 3\text{H}_2\text{O}$
Molecular weights (g/mol)	241.60 g/mol
Structural formula	
Density (g/cm ³)	2.05 g/cm ³
Company	Loba Chemie (INDIA)

2.4 Cu(II) ion adsorption experiment

This study obtained copper nitrate trihydrate from scientific equipment suppliers in Bab Al-Moatham markets, Baghdad, Iraq, with over 99.9% purity. Heavy metals properties get explained in Table 1. The preparation of copper (II) solutions utilized stock solution of Cu(II) ions starting at 1000 mg/L. A

researcher diluted the stock solution according to necessary concentration requirements. Batch adsorption experiments investigated different parameters such as temperature and pH value along with contact times and agitation speed and adsorbent dosage and initial heavy metal solution concentration. The experimental procedures were executed three times for confirming data reliability. Standard deviation analysis evaluated the experimental data for its consistency and data variability. The dispersion of the experimental data was ascertained by standard deviation analysis, guaranteeing accurate and repeatable results. The statistics were produced using the SPSS 22 program. The initial pH of the solution should be less than 8 to prevent Cu(II) precipitation during adsorption [40-42].

The batch experiments employed a magnetic stirrer (type LMS-1003) to swirl the aqueous solution during the adsorption process. A notable reduction in Cu(II) ion concentrations was observed in the solution over time. The efficiency of Cu(II) removal (%) and the adsorbent capacities (q_e , mg/g) were considered by the following formulas [43, 44].

$$\text{Copper removal}(\%) = \frac{(C_o - C_e)}{C_o} \times 100(\%) \quad (1)$$

$$\text{Adsorption capacity, } q_e = \frac{(C_o - C_e)V}{w} \quad (2)$$

where, C_o (mg/L) and C_e (mg/L) are the preliminary and final concentration of Cu(II) ion in the adsorption experiment, W is the dry membrane weight (g), C_e is the equilibrium concentrations of Cu(II) ion (mg/L), and V is the adsorbate solution volume (Liters).

3. RESULTS AND DISCUSSION

3.1 Adsorbent characterization

The physicochemical properties were analyzed using X-ray diffraction (XRD), Brunner-Emmett-Teller (BET), scanning electron microscopy (SEM), and Fourier transform infrared spectroscopy (FTIR).

To ascertain the functional groups in WH and to confirm the changes that occurred in the functional groups before and after conversion to flash graphene, the adsorbents were analyzed using a Fourier transform infrared (FTIR) spectrometer in the range of 500 to 4000 cm^{-1} . The FTIR bands of the adsorbents, as presented in Figure 3, reveal the chemical and physical changes in the molecular structures of the materials as a result of the processes it underwent [45, 46]. As clarified in Figure 3, the FTIR spectra of the material, untreated as black line and after treatment as red line, show a shift in its molecular structure and functional groups. The two new peaks appeared at 3741 cm^{-1} initially and at 3732 cm^{-1} subsequently, point towards increased O-H/N-H stretching vibrations, indicating the presence of hydroxyl or amine moiety. The change from 2938 cm^{-1} to 2912 cm^{-1} in the 3000–2800 cm^{-1} region indicates a reduction in aliphatic C-H stretching indicative of a change of the hydrocarbon system. The peaks at 1647 cm^{-1} (before) and 1617 cm^{-1} (subsequent) C=C or C=O stretching is evident, which show changes in aromatic or carbonyl functional groups. Moreover, higher intensity of peaks is observed especially in the fingerprint region (1500 – 500 cm^{-1}) after treatment at 1082 cm^{-1} , 767 cm^{-1} , and 448 cm^{-1} suggested

that there is a structural change in the inorganic component of the sample. The FTIR analysis reveals chemical and physical modifications due to the treatment, likely involving oxidation, functionalization, or water adsorption [47].

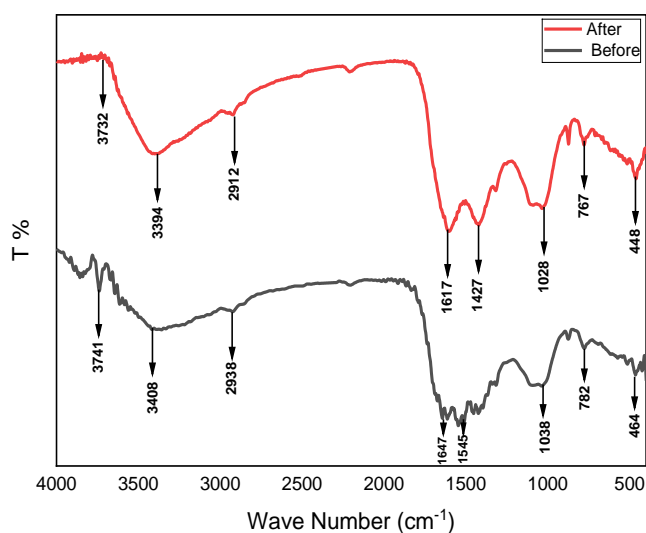


Figure 3. FTIR before and after flash joule heating

Table 2. SBET, total pore volume of before flash joule heating and after flash joule heating

Sample Label	SBET (m ² /g)	Total Pores Volume (cm ³ /g)
Before flash joule heating	24.168	0.040734
After flash joule heating	102.358	2.12

Table 2 indicates a notable increase in both the specific surfaces area (SBET) and complete pores volumes of the sample following the charring WHAF. The research shows that the adsorbent's ability to hold on to things increases as its surface area increases. This is because there are more binding sites when the surface area is more significant. Finely split solids and some porous materials can adsorb a lot of liquid [48]. The SBET rose from 24.168 m²/g before charring to 102.358 m²/g after charging, indicating a noteworthy growth in surfaces area. Correspondingly, the total pore volume escalated from 0.040734 cm³/g to 2.12 cm³/g, signifying the development of a more porous architecture. The significant rise in surface area and porosity indicates that the charring produces a highly porous and well-organized material, perhaps resulting from fast thermal expansion, evaporation of volatile substances, or reconfiguration of the material's matrix. These enhancements are essential for applications necessitating elevated surface area and porosity, like catalysis, adsorption, or energy storage systems [49].

The XRD experiment is a reliable source to show the material's characteristics accumulated which are resulting after flash joule heating process. WHBF, the material displays diffraction peaks, which were wide and low in intensity, specific for those with little to no crystallinity, higher lattice strain, and smaller crystallite size (around 7.6 the nm that is calculated by using the Scherrer equation). The XRD patterns obtained before and after flash joule heating indicated that the peaks grew more pronounced and intensified, suggesting a significant enhancement in material crystallinity (Figure 4)

[50].

An improved crystalline structure, along with the graphitization of the material, influences the adsorption mechanisms by which specific ions are adsorbed. The enhancement of crystallinity yields more stable and precisely defined surface sites, thereby improving the ion adsorption capacity, particularly for Cu(II) ions on WHAF. The diffraction peaks became sharper and more intense (e.g., a threefold increase at $2\theta = 38^\circ$), indicating a significant improvement in the material's crystallinity, alongside an increase in lattice strain and crystallite size, which reached approximately (~15.2 nm). This feature enhancement is connected to the fast, high-temperature annealing of the material during flash joule heating process, of which the rational part is that it promotes the dissolution of the amorphous regions, the new, preferred atomic configurations, and the joining of the small crystallites into larger, more ordered structures. The displacement of the peaks signals the absence of phase transitions; thus, it is apparent that the flash joule heating process actually enhances the current crystalline phase through the provision of judgments [51, 52].

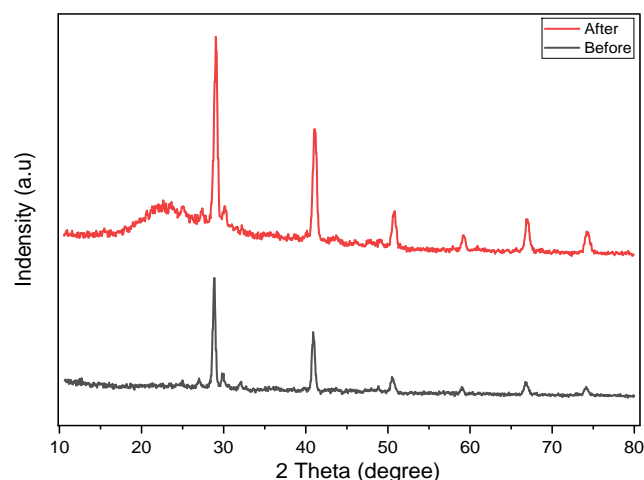


Figure 4. XRD before flash joule heating and after flash joule heating

The SEM analysis revealed that the material's surface morphology underwent substantial changes before and after flash joule heating, which was responsible for the power pulse. The surface is coarsely textured, and disordered particles merge into irregular clusters in Figure 5(a, b). On a smaller scale (1 μm), microspores and fissures, in addition to fractures and pores, are seen, which are a clear indication of crystallinity shortage and weak antiparticle adhesive forces. When observed at the 500 nm scale, small size, non-uniform distribution, and incomplete crystallinity are the main characteristics of the particles, and a rough surface is evident, which points to lots of defects on the surface. WHAF in Figure 5(c, d), the material looks smoother and less complex, and its surface becomes more homogeneous and denser. It is very clear now that at the 1 μm scale, fewer defects are leading to dense particle aggregation. On the 500 nm scale, the material is composed of well-defined crystalline structures, and the particles are quite uniform and less rough. These changes are a sign that flash joule heating eliminates imperfections, raises the level of crystallinity, and plays a more important role in the process of the aggregation of the smaller particles into bigger, well-structured grains. After the post- flash joule heating treatment, the surface became denser and more crystalline,

which not only improved the mechanical strength of the material but also provided a more consistent place for the implementation of gold nanoparticles. This improvement is especially important for Cu(II) removal purposes because it ensures strong adhesion and durability as well as the effective functioning of the nanoparticles [53, 54].

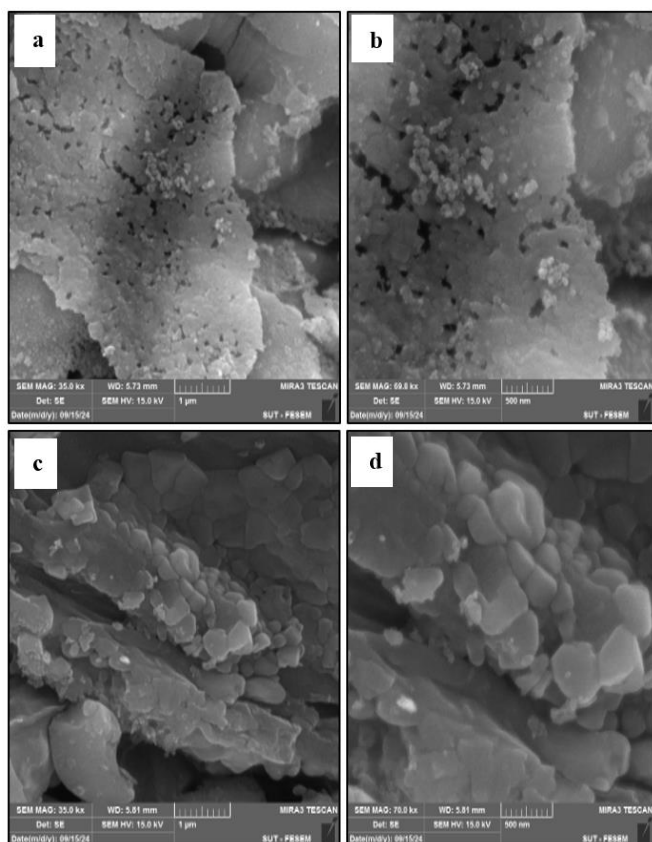


Figure 5. SEM of (a) 1 µm before flash joule heating, (b) 500 nm before flash joule heating, (c) 1 µm after flash joule heating, and (d) 500 nm after flash joule heating

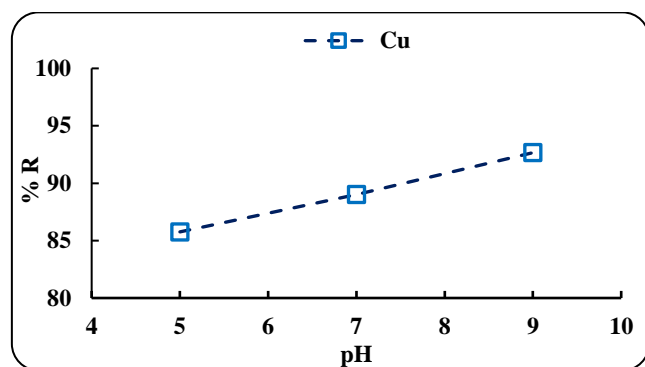


Figure 6. Effect of initial pH value on removal efficiency of Cu(II) (C_0 : 50 mg/L, contact time 60 min., adsorbent dose 0.5 g, solution vol. 100 ml)

3.2 The pH effect

The optimal pH was established by sequentially adjusting the pH of a 50 mg/L Cu(II) solution to values ranging from 5 to 9. The mixtures were agitated for one hour at ambient temperature, utilizing 0.5 g of adsorbent in a total volume of 100 ml at a speed of 150 rpm. WHAF has been utilized as a sorbent material in the testing. The primary determinant

influencing the efficacy of the adsorption system in pollutant removal is the surface appearances of the adsorbent and the properties of the adsorbate at the specified pH [55]. The studies indicate that the removal rate $R\%$ for Cu(II) peaks at 92.66% at pH = 9; however, this figure is not an accurate representation due to the handling of Cu(II) components during the precipitation phase. The optimal pH is 7, yielding exceptionally high clearance rates of 89.020. Furthermore, the results of the experiment are obtainable in Figure 6. The surface adsorption reaction occurs through the electrostatic bond formation between Cu(II) and surface functional groups with matching electrostatic potential [56].

3.3 The dosage effect

The effect of adsorbent dosage is a fundamental variable examined to assess the removal efficiency and adsorption capacity of the adsorbent material. Different levels of WHAF inclusive of 0.25; 0.5; 0.75; 1 and 1.25 g/100 ml were used in the adsorption test with 50 mg/L Cu(II) and stirred at 150 rpm. For each dosage, the adsorption value was determined, and the differences in adsorption values were analyzed. It was established that the highest Cu(II) elimination percentage was achieved when the dosage was set at 1 g. The following information is depicted graphically in Figure 7 below. Literature review also showed that while removal efficiency increases as the dose rises, the adsorption capacity decreases. The differences in removal capability and the amount of adsorbent used stem from the presence of a large number of active sites on the surface of the adsorbent, and more of these active sites are utilized when smaller amounts of the adsorbent are used [57]. Furthermore, as the amount of adsorbent material increases, the frequency of encounters between the grains of the adsorbent also increases. As a result, ions stick to the surface of the solid material. These ions may then be returned to the solution as a result of these collisions, a process called desorption. Furthermore, the anticipated amount of the adsorbent increases, layers of the materials are generated, and the adsorption sites step into competition with the ions of the pharmaceutical substances, thus reducing the adsorption capability [58].

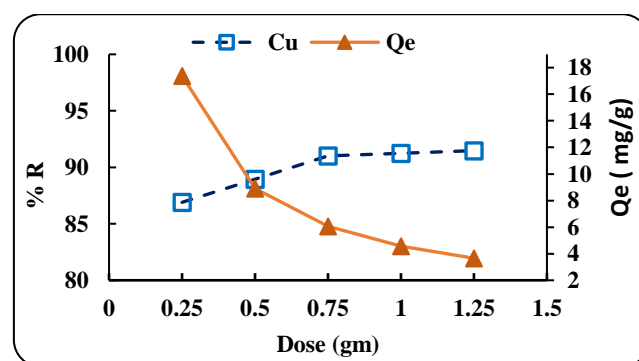


Figure 7. Influence of adsorbent dosage value on removal efficiency of Cu(II) (C_0 : 50 mg/L, pH 7, contact time 60 min., solution vol. 100 ml)

3.4 The contact time effect

The assessment of Cu(II) adsorption equilibrium occurred during different time intervals ranging from 20 minutes to 120 minutes on the modified adsorbent system. The laboratory work followed defined test parameters by using 1-gram

adsorbent samples at 50 mg/l concentration along with pH7 solutions. The modified adsorbent maintains its effective Cu(II) removal characteristics at all stages of contact time (Figure 8). Studies investigating contact time patterns show that heavy metal removal improves rapidly at first in this process. The adsorption process takes place when physical adsorption or ion exchange properties work on the solid adsorbent surface. The surface presents limited spaces where metal ions can attach during the beginning of the process period. Through time more vacant binding sites decrease until they become stagnant [59]. This research obtained its saturation curves in a short time after the beginning (20 minutes) because the biomass surface contained few active sites for metals binding. The experiment demonstrated that the best time duration for using the modified adsorbent to extract Cu(II) from aqueous solutions occurred during 60 minutes of contact duration. The delivery of maximum contaminant removal requires exceeding the specified contact time standards. During the 60-minute reaction phase the biomass attained maximum Cu(II) removal of 91.290%. The reaction rates of Cu(II) removal amounted to 91.77% and rose to 92.05% and 92.09% respectively in Figure 8. The tests involving adsorption used the maximum removal percentage recorded during the equilibrium time period of 60 minutes.

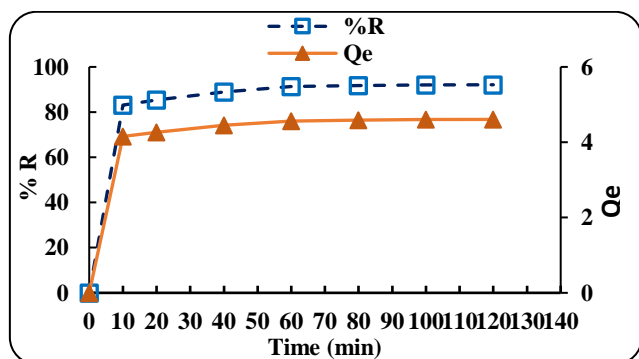


Figure 8. Impact of contact duration on the efficiency of copper removal (initial concentration: 50 mg/L, pH 7, adsorbent dose: 1 g, solution volume: 100 mL)

3.5 The initial concentration effect

Researchers evaluated how initial Cu(II) ions affected the adsorption of Cu(II) by WHAF through experiments whose results appear in Figure 9. The tests were conducted by constant WHAF dosage and contact time at 1 g 100mL⁻¹ and 100 minutes to measure removal efficiency (%) towards concentrations of 10, 20, 30, 40 and 50 mg L⁻¹ initial Cu(II) ions. The removal percentage of Cu(II) decreased from 95.44%, 93.97%, 93.45%, 93.28%, and 92.11% in Figure 9 respectively when Cu(II) ion concentration rose from 10 to 50 mg L⁻¹ during the experiment. The level of accessibility for adsorption sites provides an explanation for this finding. When the starting concentration of Cu(II) ions remains low more available adsorption sites will be accessible for binding. At elevated concentrations, the quantity of Cu(II) ions in the solution rises, resulting in the majority of Cu(II) ions remaining unabsorbed due to the saturation of adsorption sites. Due to the WHAF dosage being restricted to 1 g/100 ml, Cu(II) ions are likely to participate for the active adsorption sites of WHAF. The adsorption capacity exhibited a linear rise with the rising starting concentration of Cu(II) ions from 5 to 25 mg L⁻¹. The adsorption capacity for Cu(II) ions increased, while

the removal efficiency diminished as the starting concentrations of Cu(II) ions rose. This suggested that the elevation of initial concentrations of Cu(II) ions augmented the driving force at the solid–liquid interface, hence enhancing the adsorption capacity until the active sites accessible for Cu(II) adsorption were depleted [60]. The results demonstrated that the adsorption efficiency was directly proportional to the starting concentration of Cu(II) ions. To elucidate the adsorption behaviors comprehensively, the experimental data were further analyzed using the Freundlich and Langmuir isotherm models.

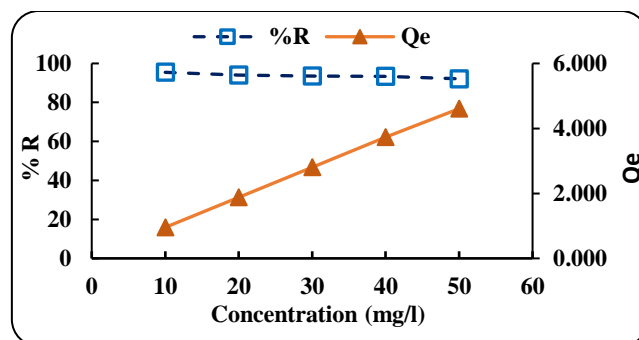


Figure 9. Influence of initial copper (II) concentration on removal efficiency (contact time: 100 min, pH: 7, adsorbent dose: 1 g, solution volume: 100 mL)

3.6 Effect of agitation speed

Figure 10 illustrates that around 92.18% of the copper was eliminated at an agitation speed of 100, with absorption increasing alongside the shaking rate. The absorption of metal ions increased progressively as the agitation speed rose from 100 to 300 rpm, resulting in the removal of approximately 94.07% of Cu(II). This can be ascribed to enhanced ion diffusion towards the surface of the reactive medium, hence facilitating adequate interaction between solution ions and binding sites [61].

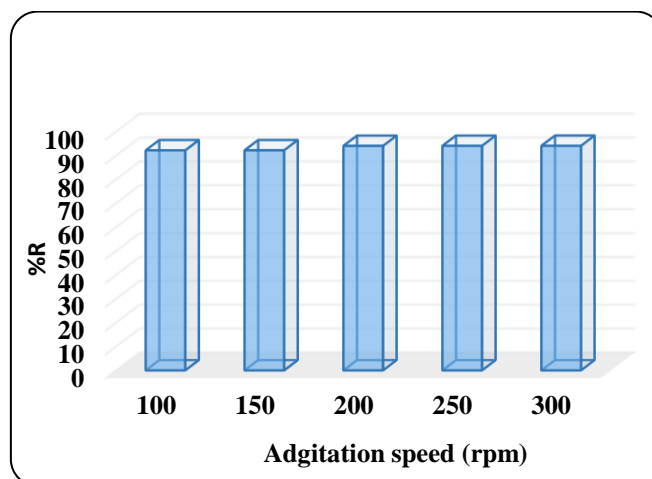


Figure 10. Impact of agitation speed on the removal efficiency of copper (II) (contact time: 100 min, pH: 7, adsorbent dose: 1 g, solution volume: 100 mL)

3.7 Temperature effect

Temperature influences adsorption in various areas, including the solubility of Cu(II) ions, the swelling capacity of

the adsorbent, and the equilibrium position related to exothermic or endothermic adsorption phenomena [62]. Temperature also influences the chemical potential of a substance. The adsorption of Cu(II) ions using WHAF adsorbent demonstrated that both the adsorption capacity and removal percentage increased with elevated reaction temperatures, as illustrated in Figure 11. The temperature rise from 25°C to 45°C resulted in an enhancement of adsorption capacity and removal percentage from 4.6 mg/g to 9.4 mg/g and from 92.07% to 94.03%, respectively. The adsorption rate was virtually uniform across all temperature treatments. Elevating the reaction temperature induces alterations in pore size, enhances the kinetic energy of Cu(II) molecules, and accelerates diffusion rates. A comparable response was documented by study [63].

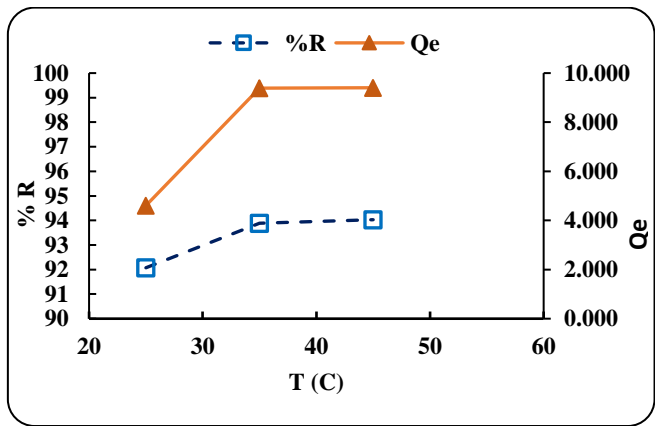


Figure 11. Influence of temperature on removal efficiency of Cu(II) (pH: 7, contact time: 100 min., solution vol.: 100 ml, adsorbent dose: 1 g)

3.8 Adsorption isotherm studies

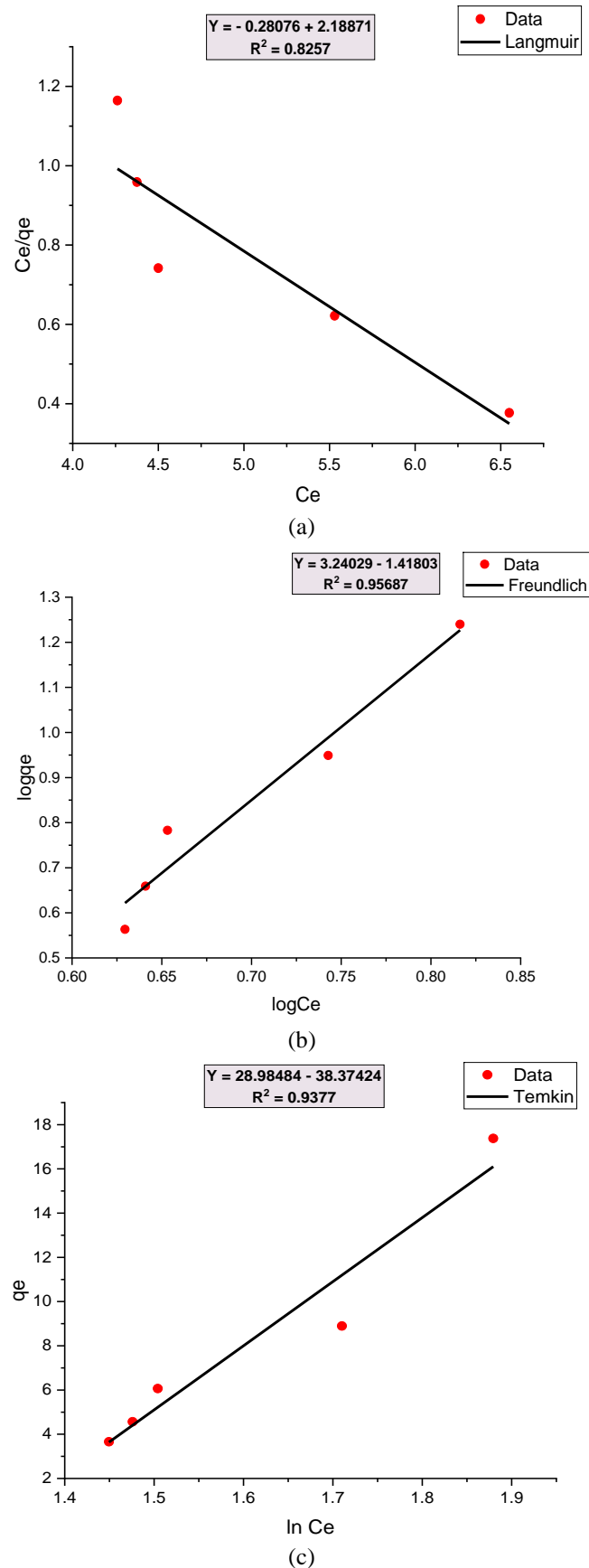
Table 3. Parameters of isotherm for removal of Cu(II) by WHAB

Isotherm Model	Parameter	Value	R ²
Langmuir	q _{max} = -3.561	mg/g	0.8257
	k _L = -0.128	L/mg	
Freundlich	K _F = 0.242	mg/g	0.9568
	n = 0.308		
Temkin	K _T = 3.758	L/mg	0.9377
	b = 85.520	J/mol	
D-R	q _{max} =290.295	mg/g	0.9518
	k = 3.00E-06	mol ² /J ²	

Equilibrium models function as important analytical instruments to study sorption mechanism processes. Our team examines the connection between the adsorbent equilibrium content with the adsorbate uptake per unit of adsorbent material under stable temperature conditions [64]. This research approved four approaches for evaluating the sorption process: Langmuir and Freundlich and Temkin and Dubinin-Radushkevich isotherm models. The adsorbent's affinity and surface characteristics along with sorption mechanism become accessible through comprehensive analysis of model parameters [65, 66]. The experimental results list parameters determined for all isotherms together with correlation coefficients R² in Table 3 and results of this analysis appear in Figure 12. The Freundlich adsorption concept applies to monolayer adsorption. The premise is that maximum adsorption equates to a saturated monolayer of solutes

molecules on the adsorbent surfaces, that the adsorption energy remains constant, and that there is no lateral migration of the adsorbate on the surface [67]. The equation for the Langmuir isotherm is:

$$q_e = \frac{q_e b C_e}{1 + b C_e} \tag{3}$$



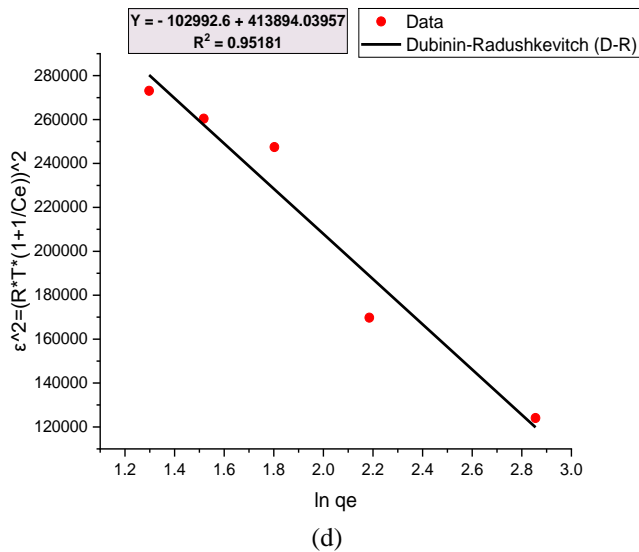


Figure 12. Linear plots of (a) Langmuir isotherm model, (b) Freundlich isotherm model (c), Temkin isotherm model, and (d) D-R isotherm model for removal of Cu(II) by WHAB

The linear form of Eq. (4) is:

$$\frac{C_e}{q_e} = \frac{1}{q_m b} + \frac{C_e}{q_m} \quad (4)$$

where, q_e represents the sorbed metal ions on the biomass (mg/g), q_m denotes the maximal sorption capacity for monolayer coverage (mg/g), b signifies the constant associated with the affinity of the binding site (L/mg), and C_e indicates the concentration of metal ions in the solution at equilibrium (mg/L). The Langmuir isotherm is predominantly employed to characterize the adsorption isotherm, constrained by the premise of uniform adsorption energies on the adsorbent's surface.

The Freundlich isotherm applies to heterogeneous surfaces [68] and is represented by Eq. (5).

$$q_e = K_F C_e^{1/n} \quad (5)$$

The two Freundlich constants K_F and n define both the adsorption capacity and intensity during this process. The Langmuir model fails to provide information regarding how much adsorbate creates a complete monolayer. The linear plot between $\ln q_e$ and $\ln C_e$ measurements will provide both K_F and $1/n$ values where F refers to the intercept of the plot [69].

Researchers base the Temkin isotherm model on a linear relationship between the heat of adsorption of all molecules as a function of layer coverage, which develops from interactions between adsorbates and results in a consistent energy binding network until it reaches a maximum binding energy. The mathematical representation of the Temkin isotherm is expressed in the following form.

$$q_e = \frac{RT}{b} \ln(K_T C_e) = B \ln(K_T C_e) \quad (6)$$

where, C_e (mg/L) denotes the pollutant concentration in solution at equilibrium. The constant B , defined as RT/b , is related to the adsorption heat, where R is the universal gas constant (8.314 J/mol·K), T is the temperatures in Kelvin, b indicates the variation in adsorption energy (J/mol), and K_T is

the equilibrium binding constant ($L \cdot mg^{-1}$), which corresponds to the maximal binding energy [70]. The Dubinin–Radushkevich (D-R) isotherm assume that the adsorbent is comparable in size to micro-pores, and the adsorption equilibrium relationship for a given adsorbate-adsorbent combination is expressed independently of temperature using the adsorption potential (ε) [71], as represented in Eq. (7).

$$\varepsilon = RT \ln \left(1 + \frac{1}{C_e} \right) \quad (7)$$

The D-R isotherm is based on a Gaussian-type distribution for the characteristic curve, and the corresponding model is expressed by Eq. (8):

$$\ln q_e = \ln q_s - B \varepsilon^2 \quad (8)$$

In this context, ε denotes the Polanyi potential, q_s is the D-R constant (mol/g), and B (mol^2/J^2) is the average free energy of sorption per mole of sorbate when transferred from infinity to the solid surface in solution. The energy is determined using the following equation:

$$E = 1/\sqrt{2B} \quad (9)$$

where, E (J/mol) represents the sorption free energy at the time of transfer from the bulk solution to the solid surfaces. Equilibrium sorption tests were conducted for Cu(II) adsorption. Samples were exposed to varying grams of adsorbent with a dissolved Cu(II) concentration of 50 (mg/L). The adsorbent was removed from the solutions after 1 hours to allow sufficient time for the adsorption process to achieve equilibrium. The isotherm model of Freundlich effectively characterized the adsorption process, exhibiting a high coefficient of determination ($R^2 = 0.956$), surpassing other models, particularly at low initial concentrations of Cu(II). The results indicate that the removal of heavy metal Cu(II) using the WHAF adsorbent is technically viable and highly efficient.

3.9 Adsorption kinetic studies

Four kinetic models were used to investigate the Cu(II) adsorption kinetics onto WHAF adsorbent: pseudo-first-order and pseudo-second-order and Elovich and intra-particle diffusion models. Experiment data served as input for applying these models to select the most suitable one [72, 73]. The evaluation required researchers to obtain rate constants together with equilibrium time measurements and equilibrium adsorption capacity values and adsorption rate calculations. The common expression of the pseudo-first-order kinetic model is as follows [74]:

$$\ln(q_e - q_t) = \ln q_e - k_1 t \quad (10)$$

where, q_e ($mg \cdot g^{-1}$) denotes the adsorption capacity at equilibrium, q_t (mg/g) represents the capacity of adsorption at time t , k_1 (min^{-1}) signifies the rate constant of the pseudo-first-order model.

The pseudo-second-order model provides an alternative kinetic framework, especially effective in systems where the rate-limiting step is chemical sorption [75].

The Eq. (11) is articulated as follows:

$$\frac{t}{q_t} = \frac{1}{K_2 q^2} + \frac{t}{q_e} \quad (11)$$

where, k_2 is the rate constant of the pseudo second-order model.

The Elovich model is used to characterize adsorption kinetics in systems with chemical sorption and a heterogeneous adsorbent surface [76]. The corresponding Eq. (12) is given below:

$$q_e = \frac{1}{\beta} \ln(\alpha\beta) + \frac{1}{\beta} \ln(t) \quad (12)$$

where, β (mg/g) represents the constant of Elovich, while α (mg/g min) denotes the preliminary adsorption rates.

The intraparticle diffusion model is commonly applied to identify the rate-controlling step in the adsorption process [77]. If the plot of the model produces a straight line passing through the origin, it suggests that intraparticle diffusion is the dominant and rate-limiting mechanism. Deviation from the linear shape shows that boundary layer mass transfer resistance starts affecting the system. The mathematical formula expresses the model as written in Eq. (13):

$$q_t = k_{diff} t^{0.5} + C_i \quad (13)$$

The influence of contact duration on the adsorption of Cu(II) onto WHAF adsorbent was examined over a period of 10 to 120 minutes following vortex agitation of the solution at ambient temperature. The data indicate that the adsorption process of Cu(II) was quick due to the presence of active adsorption sites on the WHAF adsorbent. After approximately 60 minutes, the adsorption process of Cu(II) attained equilibrium, exhibiting an adsorption capacity of 4.56 mg g^{-1} .

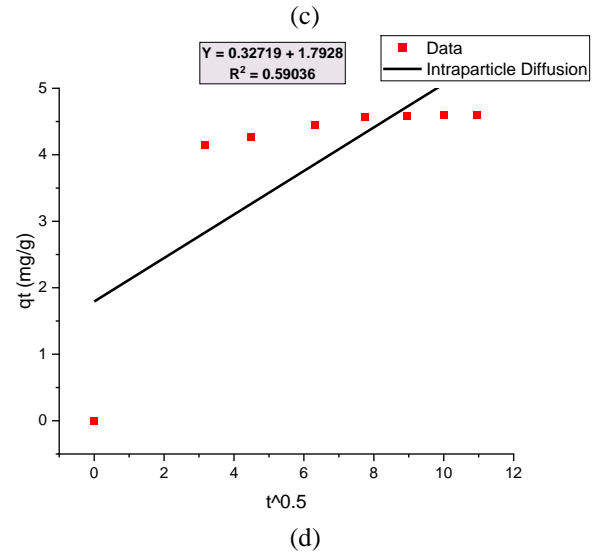
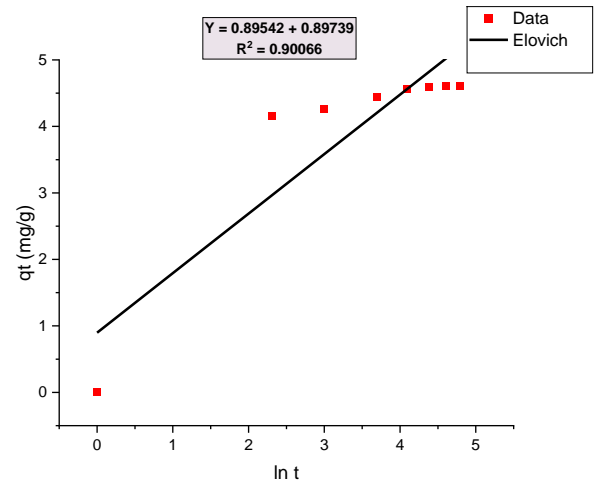
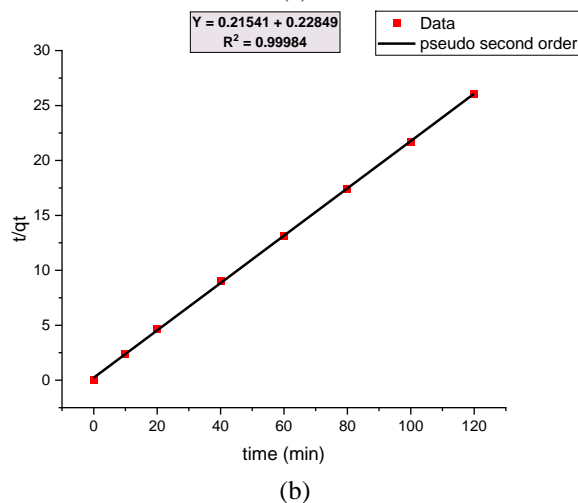
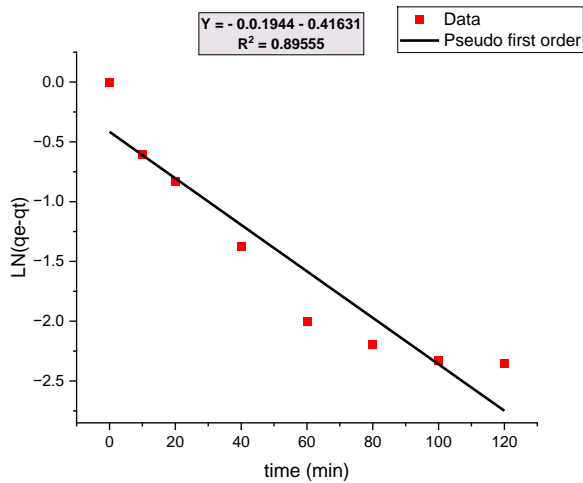


Figure 13. Linear plots of kinetics models (a) Pseudo-first order, (b) Pseudo-second order (c), Elovich, and (d) Intraparticle diffusion for removal of Cu(II) by WHAB

The adsorption kinetics were employed to explore the mechanism of copper adsorption onto the WHAF adsorbent. The experimental data were analyzed using various models, including the pseudo-first-order (Figure 13(a)), pseudo-second-order (Figure 13(b)), Elovich (Figure 13(c)), and intraparticle diffusion (Figure 13(d)) models.

Table 4. Parameter values of adsorption kinetics constants for Cu(II) Ions Removal using WHAF

Kinetic Models	Parameter	Value	R ²
Pseudo-first order	$q_e = 0.659$	mg/g	0.8955
	$k_1 = 0.019$	1/min	
Pseudo-second order	$q_e = 4.642$	mg/g	0.9998
	$k_2 = 0.203$	g/mg. min	
Elovich	$\alpha = 2.439$	mg/g. min	0.9006
	$\beta = 1.116$	g/mg	
Intraparticle diffusion	$K_{diff} = 0.327$	mg/g. min	0.5903
	$C_i = 1.792$	g/mg	

The constant parameters along with correlation coefficients from the different kinetic models used to study Cu(II) adsorption on WHAF appear in Table 4. The experimental

data exhibits improved correlation with the pseudo-second-order model while maintaining a high coefficient of determination ($R^2 = 0.999$) which demonstrates chemical sorption as the determining factor in rate-control of Cu(II) adsorption [78].

3.10 Thermodynamic studies

Adsorption was directed at three distinct temperatures (25, 35, and 45°C) to analyses adsorption thermodynamic parameters, specifically the changes in standard free energy, enthalpy, and entropy. The parameters were then computed using the following Eq. (14) [79]:

$$\Delta G^\circ = -RT \ln K_c \tag{14}$$

$$\Delta G^\circ = \Delta H^\circ - T \Delta S^\circ \tag{15}$$

where, T denotes temperatures in Kelvin, R denotes the universal gas constant (8.314 J/mol), and K_c signifies the equilibrium constant. Eq. (15) represents the equilibrium constant which describes the metal ion concentration present on the adsorbent compared to the remaining metal ion level in the solution equilibrium state.

$$K_c = \frac{q_e}{c_e} \tag{16}$$

When Eqs. (15) and (16) are combined, the vant Hoff equation is obtained:

$$\ln K_c = \frac{\Delta S^\circ}{R} - \frac{\Delta H^\circ}{RT} \tag{17}$$

Table 5. Thermo-dynamic parameters for Cu(II) adsorption onto WHAF

Adsorbate	T(C)	ln K _c	ΔG° (kJ/mol)	ΔH° (kJ/mol)	ΔS° (J/mol/K)
Cu(II)	25	0.14958499	-0.370607582	39.69935	0.135692794
	35	1.123107886	-2.87595584	39.69935	0.135692794
	45	1.14742904	-3.033632563	39.69935	0.135692794

4. CONCLUSION

Research analyzed the Cu(II) ion adsorption process that occurs on Water hyacinth flash joule heating (WHAF) through meticulous testing. Researchers employed four models namely Temkin, Freundlich, Langmuir, and Dubinin-Radushkevich equations to study equilibrium isotherm behavior. Freundlich equation delivered accurate fit to the adsorption isotherms which demonstrates heterogeneous surface adsorption phenomenon. The pseudo-second-order reaction kinetics precisely describes Cu(II) ion adsorption better than other models tested in this research including pseudo-first order and Elovich and intraparticle diffusion. In the pseudo-second order reaction kinetics, the computed value of q_e and the experimental value of q_e are closely aligned, however in other kinetic models, the discrepancy between these values is more pronounced. Moreover, the correlation coefficients are elevated in the pseudo-second order reaction kinetics. The negative ΔG values indicated that the adsorption of Cu(II) ions onto WHAF was both possible and spontaneous. The positive ΔH value signifies that the adsorption process is endothermic and the type of adsorption is chemisorptive. The positive entropy the disorder is increasing from the adsorption of

The slopes and intercept of the linear graphs of $\ln K_c$ vs $1/T$ (Figure 14) were utilized to compute the change in enthalpy (ΔH°) and entropy (ΔS°).

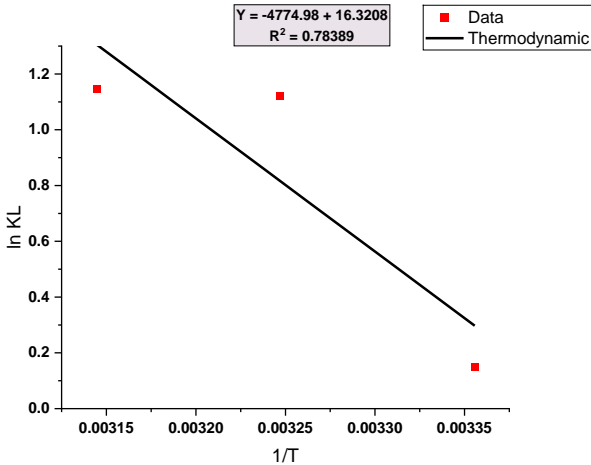


Figure 14. The plot of $\ln K_L$ vs. $1/T$ for Cu(II) sorption onto WHAF

Table 5 shows the derived thermodynamic parameters. The spontaneous nature of Cu(II) ion adsorption at the studied temperatures is evident from the negative ΔG° values. Laboratory data indicates that the absorption process occurs through chemisorption while the endothermic behavior is shown through the high positive value of ΔH° . The positive value of ΔS° shows a rise in the amount of disorder and unpredictability that emerges during metal ion adsorption on the adsorbent at the solid-solution interface [80].

metals ions on the adsorbent. Based on the outcomes, it can be inferred that WHAF is effective for the removal of Cu(II) ions from wastewater via adsorption. This WHAF offers a significant advantage by providing low-cost recovery procedures, rendering them appropriate for application.

REFERENCES

[1] Ismail, U.M., Vohra, M.S., Onaizi, S.A. (2024). Adsorptive removal of heavy metals from aqueous solutions: Progress of adsorbents development and their effectiveness. *Environmental Research*, 118562. <https://doi.org/10.1016/j.envres.2024.118562>

[2] Yu, T., Wang, J., Ding, N., Guo, X., Wang, M., Chen, Y. (2024). Tourmaline for heavy metals removal in wastewater treatment: A review. *Journal of Industrial and Engineering Chemistry*, 131: 44-53. <https://doi.org/10.1016/j.jiec.2023.10.048>

[3] Joshi, N.C., Joshi, A., Mitra, D., Gururani, P., Kumar, N., Joshi, H.K. (2024). Removal of heavy metals using cellulose-based materials: A mini-review. *Environmental Nanotechnology, Monitoring &*

- Management, 21: 100942. <https://doi.org/10.1016/j.enmm.2024.100942>
- [4] Tahir, I., Alkheraije, K.A. (2023). A review of important heavy metals toxicity with special emphasis on nephrotoxicity and its management in cattle. *Frontiers in Veterinary Science*, 10: 1149720. <https://doi.org/10.3389/fvets.2023.1149720>
- [5] Yu, H., Li, C., Yan, J., Ma, Y., Zhou, X., Yu, W., Kan, H., Meng, Q., Xie, R., Dong, P. (2023). A review on adsorption characteristics and influencing mechanism of heavy metals in farmland soil. *RSC Advances*, 13(6): 3505-3519. <https://doi.org/10.1039/d2ra07095b>
- [6] Joshi, N.C., Gururani, P. (2023). A mini review on heavy metal contamination in vegetable crops. *International Journal of Environmental Analytical Chemistry*, 1-12.
- [7] Aziz, K.H.H., Kareem, R. (2023). Recent advances in water remediation from toxic heavy metals using biochar as a green and efficient adsorbent: A review. *Case Studies in Chemical and Environmental Engineering*, 100495. <https://doi.org/10.1016/j.csee.2023.100495>
- [8] Hu, N., Lv, Y.F., Luo, B.Y., Ye, Y.C., et al. (2023). Preparation and performance of porous ceramsite for Ag⁺ removal in sewage treatment with total phosphorus tailings. *Journal of Cleaner Production*, 413: 137515. <https://doi.org/10.1016/j.jclepro.2023.137515>
- [9] Patel, P.K., Pandey, L.M., Uppaluri, R.V.S. (2024). Highly effective removal of multi-heavy metals from simulated industrial effluent through an adsorption process employing carboxymethyl-chitosan composites. *Environmental Research*, 240: 117502. <https://doi.org/10.1016/j.envres.2023.117502>
- [10] Ebrahim, S. E., Sulaymon, A.H., Alhares, H.S. (2016). Competitive removal of Cu²⁺, Cd²⁺, Zn²⁺, and Ni²⁺ ions onto iron oxide nanoparticles from wastewater. *Desalination and Water Treatment*, 57(44): 20915-20929. <https://doi.org/10.1080/19443994.2015.1112310>
- [11] Vardhan, K.H., Kumar, P.S., Panda, R.C. (2019). A review on heavy metal pollution, toxicity and remedial measures: Current trends and future perspectives. *Journal of Molecular Liquids*, 290: 111197. <https://doi.org/10.1016/j.molliq.2019.111197>
- [12] Naser, Z.A., Abdul-Hameed, H.M. (2022). Removal of Cu(II) from industrial wastewaters through locally-produced adsorbent prepared from orange peel. *Caspian Journal of Environmental Sciences*, 20(1): 45-53.
- [13] Tang, X., Fan, C.Z., Zeng, G.M., Zhong, L., et al. (2022). Phage-host interactions: The neglected part of biological wastewater treatment. *Water Research*, 226: 119183. <https://doi.org/10.1016/j.watres.2022.119183>
- [14] Wu, Z., Wang, Y.P., Xiong, Z.K., Ao, Z.M., et al. (2020). Core-shell magnetic Fe₃O₄@ Zn/Co-ZIFs to activate peroxymonosulfate for highly efficient degradation of carbamazepine. *Applied Catalysis B: Environmental*, 277: 119136. <https://doi.org/10.1016/j.apcatb.2020.119136>
- [15] Zhao, C., Zhou, J., Yan, Y., Yang, L.W., et al. (2021). Application of coagulation/flocculation in oily wastewater treatment: A review. *Science of the Total Environment*, 765: 142795. <https://doi.org/10.1016/j.scitotenv.2021.142795>
- [16] Xu, K., Li, L., Huang, Z., Tian, Z., Li, H. (2022). Efficient adsorption of heavy metals from wastewater on nanocomposite beads prepared by chitosan and paper sludge. *Science of the Total Environment*, 846, 157399. <https://doi.org/10.1016/j.scitotenv.2022.157399>
- [17] Zeng, M., Echols, I., Wang, P., Lei, S., et al. (2018). Highly biocompatible, underwater superhydrophilic and multifunctional biopolymer membrane for efficient oil-water separation and aqueous pollutant removal. *ACS Sustainable Chemistry & Engineering*, 6(3): 3879-3887. <https://doi.org/10.1021/acssuschemeng.7b04219.s001>
- [18] Xiao, Z., Zheng, Y.X., Chen, P., Liu, H., et al. (2022). Photocatalytic degradation of ciprofloxacin in freshwater aquaculture wastewater by a CNBN membrane: Mechanism, antibacterial activity, and cyclability. *Environmental Science: Nano*, 9(8): 3110-3125. <https://doi.org/10.1039/d2en00468b>
- [19] Mohammed, A., Najim, A. A., Al-Musawi, T. J., Alwared, A. I. (2019). Adsorptive performance of a mixture of three nonliving algae classes for nickel remediation in synthesized wastewater. *Journal of Environmental Health Science and Engineering*, 17: 529-538. <https://doi.org/10.1007/s40201-019-00367-w>
- [20] Neris, J.B., Luzardo, F.H.M., Santos, P.F., de Almeida, O.N., Velasco, F.G. (2019). Evaluation of single and tri-element adsorption of Pb²⁺, Ni²⁺ and Zn²⁺ ions in aqueous solution on modified water hyacinth (*Eichhornia crassipes*) fibers. *Journal of Environmental Chemical Engineering*, 7(1): 102885. <https://doi.org/10.1016/j.jece.2019.102885>
- [21] Nandiyanto, A.B.D., Ragadhita, R., Hofifah, S.N., Al Husaeni, D.F., Al Husaeni, D.N., Fiandini, M., Luckiardi, S., Soegoto, E.S., Darmawan, A., Aziz, M. (2024). Progress in the utilization of water hyacinth as effective biomass material. *Environment, Development and Sustainability*, 26(10): 24521-24568. <https://doi.org/10.1007/s10668-023-03655-6>
- [22] Kainth, S., Sharma, P., Pandey, O.P. (2024). Green sorbents from agricultural wastes: A review of sustainable adsorption materials. *Applied Surface Science Advances*, 19: 100562. <https://doi.org/10.1016/j.apsadv.2023.100562>
- [23] Rashid, M., Alwared, A.I., Abdelkareem, H.N. (2023). Biosorption of Cd (II) ions by *Chlorella* microalgae: Isotherm, kinetics processes and biodiesel production. *Desalination and Water Treatment*, 311: 67-75. <https://doi.org/10.5004/dwt.2023.29990>
- [24] Mengist, Y., Moges, Y. (2019). Distribution, impacts and management option for water hyacinth (*Eichhornia crassipes* [Mart.] Solms) in Ethiopia: A review. *Journal of Advances in Agriculture*, 10: 1764-1771. <https://doi.org/10.24297/jaa.v10i0.8308>
- [25] Xu, Z., Xing, Y., Ren, A., Ma, D., Li, Y., Hu, S. (2020). Study on adsorption properties of water hyacinth-derived biochar for uranium (VI). *Journal of Radioanalytical and Nuclear Chemistry*, 324: 1317-1327. <https://doi.org/10.1007/s10967-020-07160-2>
- [26] Banerjee, S., Sivamani, S., Namdeti, R., Prasad, B.S.N. (2023). Optimization of biomethanation of water hyacinth (*Eichhornia crassipes*) using biocatalyst. *Cellulose*, 30(5): 2883-2894. <https://doi.org/10.1007/s10570-023-05076-0>
- [27] Kumar, V., Singh, J., Kumar, P. (2020). Regression models for removal of heavy metals by water hyacinth (*Eichhornia crassipes*) from wastewater of pulp and paper processing industry. *Environmental Sustainability*,

- 3(1): 35-44. <https://doi.org/10.1007/s42398-019-00093-x>
- [28] Mishra, S., Maiti, A. (2017). The efficiency of *Eichhornia crassipes* in the removal of organic and inorganic pollutants from wastewater: A review. *Environmental Science and Pollution Research*, 24: 7921-7937. <https://doi.org/10.1007/s11356-016-8357-7>
- [29] Joshi, N., Tomar, R.K., Kumari, M., Khatri, S. (2019). Integrated water hyacinth control and waste management plan: A case of Futala Lake, Nagpur. In *Advances in Waste Management: Select Proceedings of Recycle 2016*, pp. 185-202. https://doi.org/10.1007/978-981-13-0215-2_13
- [30] Rezaia, S., Ponraj, M., Talaiekhazani, A., Mohamad, S.E., Din, M.F.N., Taib, S.M., Sairan, F.M. (2015). Perspectives of phytoremediation using water hyacinth for removal of heavy metals, organic and inorganic pollutants in wastewater. *Journal of Environmental Management*, 163: 125-133. <https://doi.org/10.1016/j.jenvman.2015.08.018>
- [31] Omran, B.A., Baek, K.-H. (2022). Valorization of agro-industrial biowaste to green nanomaterials for wastewater treatment: Approaching green chemistry and circular economy principles. *Journal of Environmental Management*, 311: 114806. <https://doi.org/10.1016/j.jenvman.2022.114806>
- [32] Sharma, A., Aggarwal, N.K. (2020). Water hyacinth: A potential lignocellulosic biomass for bioethanol. In *Water Hyacinth: A Potential Lignocellulosic Biomass for Bioethanol*. Springer. https://doi.org/10.1007/978-3-030-35632-3_7
- [33] Zhu, X., Lin, L., Pang, M., Jia, C., et al. (2024). Continuous and low-carbon production of biomass flash graphene. *Nature Communications*, 15(1): 3218. <https://doi.org/10.1038/s41467-024-47603-y>
- [34] Chinwatpaiboon, P., Savarajara, A., Luengnaruemitchai, A. (2023). Enzymatic hydrolysate of water hyacinth with NaOH pretreatment for biobutanol production via ABE fermentation by *Clostridium beijerinckii* JCM 8026. *Biomass and Bioenergy*, 173: 106782. <https://doi.org/10.1016/j.biombioe.2023.106782>
- [35] Lewoyehu, M. (2021). Comprehensive review on synthesis and application of activated carbon from agricultural residues for the remediation of venomous pollutants in wastewater. *Journal of Analytical and Applied Pyrolysis*, 159, 105279. <https://doi.org/10.1016/j.jaap.2021.105279>
- [36] Ramírez, J., Yépez, E., Pantoja-Suárez, F., Acurio, E., Pérez, F., Basile, L. (2023). Design and construction of a high-current capacitor bank for flash graphene synthesis. *Engineering Proceedings*, 47(1): 18. <https://doi.org/10.3390/engproc2023047018>
- [37] Raheem, N.S., Abdul-Hameed, H.M. (2024). Ground water remediation using flash graphene produced from banana peels: Batch mode. *International Journal of Environmental Impacts*, 7(2): 319-327. <https://doi.org/10.18280/ije.070216>
- [38] Al-Mousawi, R.A., Saeed, A.A., Al-Kadhemy, M.F., Abbas, K.N. (2023). Degradation of organically polluted water by photocatalysis of SnO₂: CuO nanocomposite under the influence of sunlight. *Mustansiriyah Journal of Pure and Applied Science*, 1(3): 103-121. <https://doi.org/10.47831/mjpas.v1i3.54>
- [39] Katiyar, R., Patel, A.K., Nguyen, T.-B., Singhanian, R.R., Chen, C.-W., Dong, C.-D. (2021). Adsorption of copper (II) in aqueous solution using biochars derived from *Ascophyllum nodosum* seaweed. *Bioresource Technology*, 328: 124829. <https://doi.org/10.1016/j.biortech.2021.124829>
- [40] Pal, D.B., et al. (2021). Low-cost biochar adsorbents prepared from date and delonix regia seeds for heavy metal sorption. *Bioresource Technology*, 339: 125606. <https://doi.org/10.1016/j.biortech.2021.125606>
- [41] Cherono, F., Mburu, N., Kakoi, B. (2021). Adsorption of lead, copper and zinc in a multi-metal aqueous solution by waste rubber tires for the design of single batch adsorber. *Heliyon*, 7(11). <https://doi.org/10.1016/j.heliyon.2021.e08254>
- [42] Abd AL-Hussain, Z.K., Abdul-Hameed, H.M. (2023). Removal of lead ions from wastewater by using a local adsorbent from charring tea wastes. *Iraqi Journal of Chemical and Petroleum Engineering*, 24(3): 93-102. <https://doi.org/10.31699/ijcpe.2023.3.9>
- [43] Mohsen, H.A., Ghanim, A.N. (2024). Removal of copper and zinc metal ions from industrial effluents in continuous mode using modified date pits. *Iraqi Journal of Chemical and Petroleum Engineering*, 25(2): 139-150. <https://doi.org/10.31699/ijcpe.2024.2.13>
- [44] Reza, M.S., Afroze, S., Bakar, M.S.A., Saidur, R., Aslfattahi, N., Taweekun, J., Azad, A.K. (2020). Biochar characterization of invasive *Pennisetum purpureum* grass: Effect of pyrolysis temperature. *Biochar*, 2: 239-251. <https://doi.org/10.1007/s42773-020-00048-0>
- [45] Elnour, Y., Alghyamah, A.A., Shaikh, H.M., Poulouse, A.M., Al-Zahrani, S.M., Anis, A., Al-Wabel, M.I. (2019). Effect of pyrolysis temperature on biochar microstructural evolution, physicochemical characteristics, and its influence on biochar/polypropylene composites. *Applied Sciences*, 9(6): 1149. <https://doi.org/10.3390/app9061149>
- [46] Mardani, M., Wang, J., Miao, W., Wang, Z. (2018). Phase equilibria in the Fe-Ce-C system at 1100°C. *Journal of Alloys and Compounds*, 730: 352-359.
- [47] Zhang, X., Chen, W., Huang, H., Zhang, L. (2024). Deep purification of copper from zinc sulfate solution using controllable aging FeS nanoparticles through slow-release sulfide precipitation. *Journal of Physics: Conference Series*, 2738(1): 12014. <https://doi.org/10.1088/1742-6596/2738/1/012014>
- [48] Liu, X., Luo, H. (2024). Preparation of coal-based graphene by flash joule heating. *ACS Omega*, 9(2): 2657-2663. <https://doi.org/10.1021/acsomega.3c07438>
- [49] Emenike, E.C., Adeniyi, A.G., Omuku, P.E., Okwu, K.C., Iwuzor, K.O. (2022). Recent advances in nano-adsorbents for the sequestration of copper from water. *Journal of Water Process Engineering*, 47, 102715. <https://doi.org/10.1016/j.jwpe.2022.102715>
- [50] De Rosa, S., Colantoni, E., Branchini, P., Orestano, D., et al. (2024). Morphological and chemical changes in nuclear graphite target under vacuum and high-temperature conditions. *Heliyon*, 10(12): e32718. <https://doi.org/10.1016/j.heliyon.2024.e32718>
- [51] Römer, F., Ramasamy, P., Steffny, I., et al. (2025). Crystallization of Fe₇₄Mo₄P₁₀C_{7.5}B_{2.5}Si₂ metallic glass: Insights from in-situ synchrotron diffraction and Flash DSC. *Materials Today Advances*, 25: 100550. <https://doi.org/10.1016/j.mtadv.2024.100550>
- [52] Hummadi, K.K. (2021). Optimal operating conditions

- for adsorption of heavy metals from an aqueous solution by an agriculture waste. *Iraqi Journal of Chemical and Petroleum Engineering*, 22(2): 27-35. <https://doi.org/10.31699/ijcpe.2021.2.4>
- [53] Vickers, N.J. (2017). Animal communication: When I'm calling you, will you answer too? *Current Biology*, 27(14): R713-R715. <https://doi.org/10.1016/j.cub.2017.05.064>
- [54] Shang, Z., Hu, Z., Huang, L., Guo, Z., Liu, H., Zhang, C. (2020). Removal of amoxicillin from aqueous solution by zinc acetate modified activated carbon derived from reed. *Powder Technology*, 368: 178-189. <https://doi.org/10.1016/j.powtec.2020.04.055>
- [55] Khan, Z.H., Gao, M., Qiu, W., Islam, M.S., Song, Z. (2020). Mechanisms for cadmium adsorption by magnetic biochar composites in an aqueous solution. *Chemosphere*, 246: 125701. <https://doi.org/10.1016/j.chemosphere.2019.125701>
- [56] Dulla, J.B., Tamana, M.R., Boddu, S., Pulipati, K., Srirama, K. (2020). Biosorption of copper (II) onto spent biomass of *Gelidiella acerosa* (brown marine algae): Optimization and kinetic studies. *Applied Water Science*, 10(2): 56. <https://doi.org/10.1007/s13201-019-1125-3>
- [57] Radha, E., Gomathi, T., Sudha, P.N., Latha, S., Ghfar, A.A., Hossain, N. (2021). Adsorption studies on removal of Pb (II) and Cd (II) ions using chitosan-derived copolymeric blend. *Biomass Conversion and Biorefinery*, 1-16. <https://doi.org/10.1007/s13399-021-01918-8>
- [58] Ke, F., Peng, C., Zhang, T., et al. (2018). Fumarate-based metal-organic frameworks as a new platform for highly selective removal of fluoride from brick tea. *Scientific Reports*, 8(1): 939. <https://doi.org/10.1038/s41598-018-19277-2>
- [59] Alwared, I., Sadiq, N.A. (2019). Competitive removal of lead, copper, and cadmium ions by sorptive flotation using marble wastes. *International Journal of Environmental Waste Management*, 23(2): 156-178. <https://doi.org/10.1504/ijewm.2019.10018025>
- [60] Arnata, W., Suprihatin, S., Fahma, F., Richana, N., Sunarti, T.C. (2019). Adsorption of anionic Congo red dye by using cellulose from sago frond. *Pollution Research*, 38(3): 43-53. <https://doi.org/10.13005/ojc/35specialissue102>
- [61] Wang, X., Jiang, S., Cui, S., Tang, Y., Pei, Z., Duan, H. (2019). Magnetic-controlled aerogels from carboxylated cellulose and MnFe_2O_4 as a novel adsorbent for removal of Cu(II). *Cellulose*, 26: 5051-5063. <https://doi.org/10.1007/s10570-019-02444-7>
- [62] Shimizu, S., Matubayasi, N. (2023). Understanding sorption mechanisms directly from isotherms. *Langmuir*, 39(17): 6113-6125. <https://doi.org/10.1021/acs.langmuir.3c00256>
- [63] Azizian, S., Eris, S. (2021). Adsorption isotherms and kinetics. In *Interface Science and Technology*, 33: 445-509. <https://doi.org/10.1016/b978-0-12-818805-7.00011-4>
- [64] Mhawesh, T.H., Abd Ali, Z.T. (2020). Reuse of brick waste as a cheap-sorbent for the removal of nickel ions from aqueous solutions. *Iraqi Journal of Chemical and Petroleum Engineering*, 21(2): 15-23. <https://doi.org/10.31699/ijcpe.2020.2.3>
- [65] Van, H.T., Nguyen, L.H., Dang, N.V., Chao, H.-P., Nguyen, Q.T., Nguyen, T.H., Nguyen, T.B.L., Thanh, D.V., Nguyen, H.D., Thang, P.Q., Thanh, P.T.H., Hoang, V.P. (2021). The enhancement of reactive red 24 adsorption from aqueous solution using agricultural waste-derived biochar modified with ZnO nanoparticles. *RSC Advances*, 11(10): 5801-5814. <https://doi.org/10.1039/d0ra09974k>
- [66] Tounsadi, H., Khnifira, M., Khalidi, A., Abdennouri, M., Barka, N. (2025). Effective removal of heavy metals from aqueous solutions using activated biomass: Analytical interpretation via molecular dynamic simulation, mathematical, and statistical approaches. *Journal of Molecular Structure*, 1319: 139371. <https://doi.org/10.1016/j.molstruc.2024.139371>
- [67] Abdulmumini, H., Ayuba, A.M. (2022). Reclamation of spent solid matrices used in adsorption of malachite green and methyl violet dyes from aqueous solution. *Journal of Materials and Environmental Science*, 13(06): 723-731.
- [68] Chu, K.H. (2021). Revisiting the Temkin isotherm: Dimensional inconsistency and approximate forms. *Industrial & Engineering Chemistry Research*, 60(35): 13140-13147. <https://doi.org/10.1021/acs.iecr.1c01788>
- [69] Bonilla-Petriciolet, A., Mendoza-Castillo, D.I., Reynel-Ávila, H.E. (2017). Adsorption Processes for Water Treatment and Purification. Springer. <https://doi.org/10.1007/978-3-319-58136-1>
- [70] Ali, A., Abdul-Hameed, H.M. (2024). Synthesis and characterization of magnetic activated carbon manufactured from palm stones by physical activation to remove lead from aqueous solution. *Desalination and Water Treatment*, 100951. <https://doi.org/10.1016/j.dwt.2024.100951>
- [71] Bojana. (2020). Guidelines for general adsorption kinetics modeling. *Hemijaska Industrija*, 74(1): 65.
- [72] Denesa, E.M., Laysandra, T., Edi Soetaredjo, F., et al. (2024). Binary adsorption kinetics of tetracycline and doxycycline on HKUST-1: Modification pseudo-first and second-order models. *Engineering Chemistry*, 8: 31-40. <https://doi.org/10.4028/p-3vojww>
- [73] Gharaghani, M.A., Samaei, M., Mahdizadeh, H., et al. (2024). An effective magnetic nanobiocomposite: Preparation, characterization, and its application for adsorption removal of p-nitroaniline from aquatic environments. *Environmental Research*, 246: 118128. <https://doi.org/10.1016/j.envres.2024.118128>
- [74] Nithya, R., Thirunavukkarasu, A., Sivasankari, C. (2023). Comparative profile of green and chemically synthesized nanomaterials from bio-hydrometallurgical leachate of e-waste on crystal violet adsorption kinetics, thermodynamics, and mass transfer and statistical models. *Biomass Conversion and Biorefinery*, 13(18): 17197-17221. <https://doi.org/10.1007/s13399-021-02269-0>
- [75] Allahkarami, E., Maleki, S., Azadmehr, A., Aghayan, S., Allahkarami, E. (2025). Fabricating nepheline syenite-chitosan composite for heavy metals uptake: Mechanism insight via statistical physics modeling. *Separation and Purification Technology*, 354: 129152. <https://doi.org/10.1016/j.seppur.2024.129152>
- [76] Bişgin, T., Gezici, O. (2022). Modelling the kinetics of direct Cu(II) adsorption on two porous resins modified with mussel-inspired chemistry. *Journal of Polymer Research*, 29: 1-19. <https://doi.org/10.1007/s10965-021-02865-8>
- [77] Yadav, S., Yadav, A., Sharma, N., Sharma, A.K., Kumar,

- S. (2024). Utilization of citric acid functionalized lignocellulosic biomass as a novel adsorbent for efficient removal of cationic dyes in single and multicomponent systems. *Cellulose*, 1-32. <https://doi.org/10.1007/s10570-024-06302-z>
- [78] Kuśmerek, K., Świątkowski, A., Zienkiewicz-Strzałka, M., Deryło-Marczewska, A. (2025). Studies of the kinetics and isotherms of copper ions adsorption on APTES-modified silica materials. *Desalination and Water Treatment*, 321: 100965.
- [79] Wang, J., Zhang, W. (2021). Evaluating the adsorption of Shanghai silty clay to Cd (II): Pb (II): As (V): and Cr (VI): Kinetic, equilibrium, and thermodynamic studies. *Environmental Monitoring and Assessment*, 193(3): 131. <https://doi.org/10.1007/s10661-021-08904-7>
- [80] Sidiali, F., Souag, R., Seddiki, N. (2023). Modeling isotherm and mechanism adsorption of heavy metals from water using brut keratin powder prepared from Algerian sheep horns. *Desalination and Water Treatment*, 307: 140-152. <https://doi.org/10.5004/dwt.2023.29900>